RSC Advances

ROYAL SOCIETY OF CHEMISTRY

www.rsc.org/advances

Controllable Wet Synthesis of Multicomponent Copper-Based Catalysts for Rochow Reaction

Yanzhao Zhai,[a, b] Yongjun Ji,*[, a] Guangna Wang,[a]

Yongxia Zhu,[a] Hezhi Liu,[a] Ziyi Zhong[c] and Fabing Su*[, a]

[a] *State Key Laboratory of Multiphase Complex Systems, Institute of Process Engineering, Chinese Academy of Sciences, Beijing, China 100190*

[b] *School of Chemical and Environmental Engineering, China University of Mining and Technology(Beijing)，Beijing, China 100083*

[c] *School of Chemical & Biomedical Engineering, Nanyang Technological University, 62 Nanyang Drive, Singapore 637459*

*To whom correspondence should be addressed. E-mail address: yjji@ipe.ac.cn (Y. Ji), fbsu@ipe.ac.cn (F. Su), Tel.: +86-10-82544850, Fax: +86-10-82544851.

Abstract

This work aims to provide a facile, low-cost and scalable method for the preparation of the multicomponent Cu-Cu_2O-CuO catalysts which are highly interested by the organosilane industry. A series of submicrometer-sized and Cu-based catalysts containing CuO, Cu_2O and Cu or some of them have been synthesized by a simple low-temperature wet chemical method using $CuSO_4 \cdot 5H_2O$ as the precursor and $N_2H_4 \cdot H_2O$ as reducing agent. The samples were characterized by X-ray diffraction, thermogravimetric analysis, temperature-programmed reduction, X-ray photoelectron spectroscopy, transmission electron microscopy, and scanning electron microscopy techniques. It was observed that the composition of the samples could be tailored by varying the amount of reducing agent at the given reaction temperature and time. These catalysts were then tested for the Rochow reaction using silicon powder and methyl chloride (MeCl) as reactants to produce dimethyldichlorosilane (M2), which is the most important organosilane monomer in the industry. Comparing with the bare CuO and Cu particles, the ternary CuO-Cu_2O-Cu catalyst displayed much improved M2 selectivity and Si conversion, which can be attributed to the smaller copper particle size and the synergistic effect among the different components in the CuO-Cu_2O-Cu catalyst. This catalyst preparation method is expected to yield efficient and low-cost copper catalysts for organosilane industry.

Keywords: Controlled synthesis; Wet chemical method; Copper-based catalysts; Rochow reaction

1. Introduction

The Rochow reaction, which was discovered in the 1940s,[1] is still the most economical route to produce silicone monomers in the organosilane industry. In this reaction, gaseous methyl chloride (MeCl) reacts with silicon (Si) in the presence of Cu-based catalysts and a trace amount of promoters as following:[2,3]

$$\mathrm{Si + MeCl} \xrightarrow[300\text{-}350\ ^{o}\mathrm{C}]{\text{Copper catalyst}} \begin{array}{c}(CH_3)_3SiCl\\(CH_3)_2SiCl_2\\CH_3SiCl_3\\CH_3HSiCl_2\\(CH_3)_2HSiCl\\\text{other low boilers}\\\text{residue}\end{array} \qquad (1)$$

Among the products from the above Rochow reaction, dimethyldichlorosilane ($(CH_3)_2SiCl_2$, M2) is the most important monomer used for silicon rubber production in organosilane industry, and thus a high M2 yield is highly desired. Besides the accurate control of reaction conditions and selection of proper reactors, development of highly efficient catalyst systems is crucial for a high M2 selectivity and Si conversion. As reported，the primary catalysts used in the Rochow reaction are Cu-based catalysts including metallic Cu,[1] CuCl,[4] Cu_2O,[5] CuO,[6] Cu-Si alloy[7] and Cu-Cu_2O-CuO,[8] together with some catalyst promoters.[2,6,9-11] In recent years, our group has developed a number of cupreous and copper oxide structures, such as flower-like ZnO grown on urchin-like CuO microspheres,[12] porous cubic Cu microparticles,[13] mesoporous Cu_2O microspheres,[5] shape-controlled Cu_2O microparticles,[14] dandelion-like CuO microspheres,[15] flower-like CuO microspheres,[16] and CuCl microcrystals with different morphologies[17] etc., for M2 synthesis, and found that the particle morphology and size as well as the catalyst composition impact on the catalytic properties significantly.

Among various Cu-based catalysts, the multicomponent Cu-based catalysts containing Cu, Cu_2O, and CuO are of great interest due to their superior catalytic performances in Rochow reaction. For instance, Khitouni et al prepared such kind of catalysts through a high-energy mechanical milling process using Cu, Cu_2O, and CuO as the precursors.[18] Although their method is simple, it still lacks effective controls on the solid reaction among Cu, Cu_2O, and CuO during the mechanical milling process. Therefore, to meet industrial application, more effective methods for preparing multicomponent Cu-based catalysts should be developed. More recently, we found that the multicomponent Cu-Cu_2O-CuO catalyst can also be synthesized by partial reduction of CuO nanoparticles in H_2/N_2 gas[19] or by controlled oxidation of copper flakes in O_2/N_2 gas.[20] These methods, however, still suffer from the low yields and use of high-cost equipment together with intensive energy consumption (high temperature), which are troublesome and thus limit their further application. On the other hand, we have noticed that there are scarce reports concerning about the preparation of multicomponent Cu-based catalysts via wet chemical approaches.

Herein, we report a facile and low cost preparation of the ternary CuO-Cu_2O-Cu catalyst by wet chemical method with obvious advantages such as mild reaction condition (70 ^oC), large-scale production capability and easy operation. Most importantly, the composition of the samples could be tailored by simply varying the amount of $N_2H_4 \cdot H_2O$ as reducing agent. The prepared ternary CuO-Cu_2O-Cu catalyst exhibited highly improved M2 selectivity and Si conversion in the Rochow reaction in comparison to those of sole CuO and Cu microparticles, demonstrating the importance of the synergistic catalytic effect among the multicomponents. The resulting ternary CuO-Cu_2O-Cu using the present method is a promising catalyst for industrial Rochow reaction.

2. Experimental

2.1. Material synthesis

The samples were synthesized using a wet chemical reduction method as shown in Fig.1. In a typical preparation, 37.5 g of copper (II) sulfate pentahydrate ($CuSO_4 \cdot 5H_2O$, A.R., Sinopharm Chemical Reagent Co., Ltd., China) was dissolved in 300.0 mL of deionized water to get a clear solution with a copper concentration of 0.5 M. Upon heating to 70 ^oC under magnetic stirring, sodium hydroxide (NaOH, A.R., Sinopharm Chemical Reagent Co., Ltd.) aqueous solution (6 M) was added dropwise until the pH value of the solution reached 7.5. The obtained mixed gel was maintained for 10 min at this temperature to give a black precipitate. Subsequently, the desired amounts of hydrazine hydrate ($N_2H_4 \cdot H_2O$) used as the reductant were introduced dropwise. After stirred for another 90 min, the reaction mixture was cooled down to room temperature naturally. The resulting solid was collected by filtration, washed with deionized water and ethanol for several times, and finally dried in a vacuum at 60 ^oC for 8 h. The synthesis was carried out by fixing the Cu amount at 9.5 g while varying the amount of $N_2H_4 \cdot H_2O$ added. The sample compositions were determined by XRD analysis, and the prepared samples are thus denoted as CuO, CuO-Cu_2O, CuO-Cu_2O-Cu, Cu_2O-Cu and Cu according to their measured compositions when the amount of $N_2H_4 \cdot H_2O$ was 0, 1.5, 2.5, 3.5 and 5.0 mL, respectively.

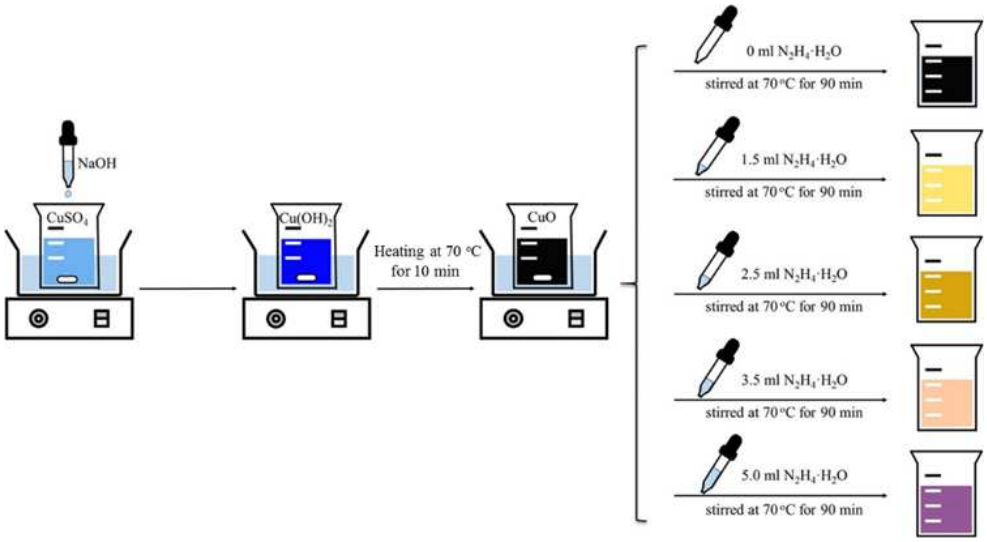

Fig. 1 Schematic illustration for the preparation process

2.2. Characterization

X-ray diffraction (XRD) patterns were recorded on a PANalytica X'Pert PRO MPD using the Kα radiation of Cu (λ = 1.5418 Å) and checked with the card number of Joint Committee on Powder Diffraction Standards (JCPDS). The crystallite size was calculated using the Scherrer equation, in which the shape factor of K is 0.90. Moreover, the 2θ value of instrumental broadening is 0.06, which was subtracted in the test process. The microscopic feature of the samples was observed by field-emission scanning electron microscopy (SEM) (JSM-7001F, JEOL, Tokyo, Japan) with energy-dispersive spectroscopy (EDS) (INCA X-MAX, JEOL, Oxford, England) and transmission electron microscopy (TEM) (JEM-2010F, JEOL, Tokyo, Japan). The specific surface area was determined according to the Brunauer−Emmett−Teller (BET) method in the relative pressure range of 0.05-0.2. Thermal gravimetric (TG) analysis was carried out on an EXSTAR TG/DTA 6300 (Seiko Instruments, Japan) with a heating rate of 10 °C/min in air (200 mL/min). H_2-temperature programmed reduction (H_2-TPR) measurements were carried out on automated chemisorption analyzer (ChemBET pulsar TPR/TPD, Quantachrome). Upon loading of about 0.10 g of sample into a quartz U-tube, the sample was degassed at 150 °C for 30 min under helium. When the temperature decreased to 30 °C, the gas was changed to 9.9 % O_2/He. Finally, the sample was heated from 30 to

900 °C at a rate of 10 °C/min in 9.9 % O_2/He with a gas flow of 30 mL/min. X-ray photoelectron spectroscopy (XPS) analysis was carried out on an ESCALAB 250Xi from Thermo Scientific Corporation using AlKa X-ray radiation.

2.3. Catalytic Measurement

The evaluation of catalyst was carried out on a homemade lab fixed-bed reactor. 10.0 g Si powder (20-50 mesh, provided by Jiangsu Hongda New Material Co., Ltd.) and 1.0 g of prepared catalyst together with 0.10 g of Zinc (Zn, A.R., Sinopharm Chemical Reagent Co., Ltd.) used as a promoter were mixed homogeneously to form a contact mass, which was loaded in the glass reactor. The reactor system was purged with high purity N_2 for 0.5 h followed by heating to 325 °C within 1 h under a N_2 flow rate of 25 mL/min. Subsequently, it was switched to the MeCl gas with a flow rate of 25 mL/min to react with Si at 325 °C. After 24 h, the reaction was ceased. The gas products were cooled with a circulator bath controlled at 5 °C by a programmable thermal circulator (GDH series, Ningbo xinzhi biological technology Co., LTD) and then identified by gas chromatography mass spectrometry (GC−MS) (QP2010, SHIMADZU), which are composed of methyltricholorsilane (CH_3SiCl_3, M1), dimethyldichlorosilane ($(CH_3)_2SiCl_2$, M2), trimethylchlorosilane ($(CH_3)_3SiCl$, M3), methyldichlorosilane (CH_3SiHCl_2, M1H), dimethylchlorosilane ($(CH_3)_2SiHCl$, M2H), low boiler (LB) and high boiler (HB). They were quantitative analyzed on a gas chromatograph (Agilent Technologies 7890A, Thermal conductivity detector, KB-201 column). Following the previously reported method,[13] the selectivity of the products was calculated by the peak area ratio (in percentage) and the Si conversion was obtained from the difference of contact masses (before and after reaction), as expressed as follows:

$$\text{Conversion of Si (C-Si)} = \frac{\text{weight (contact mass before reaction)-weight (contact mass after reaction)}}{\text{weight (Si before reaction)}} \times 100\,\% \quad (2)$$

3. Results and discussion

3.1. Characterizations of Cu-based catalysts

Fig. 2a shows the XRD patterns of all the samples, which have high diffraction intensities, indicating their good crystallinity. In the absence of $N_2H_4 \cdot H_2O$, diffraction peaks at 2θ values of 33.5°, 35.5°, 38.2°, 48.7°, 54.2°, 58.3°, 62.5°, 66.4°, 68.2°, 73.4°, and 75.6° are observed for the product, which correspond respectively to the lattice planes of (110), (−111), (111), (−202), (020), (202), (−113), (−311), (220), (311), and (004) of monoclinic CuO (JCPDS No. 03-065-2309). As compared to those of CuO, the sample prepared with 1.5mL of $N_2H_4 \cdot H_2O$ has additional diffraction peaks at 2θ=36.7° and 42.7°, which are attributed to the (111) and (200) planes of cubic Cu_2O (JCPDS No. 00-001-1142), suggesting the formation of a bicomponent system of CuO and Cu_2O. By increasing the amount of $N_2H_4 \cdot H_2O$ to 2.5 mL, in addition to the above CuO-Cu_2O diffraction peaks, new peaks at 2θ values of 43.3°, 50.5°, and 74.2° are appeared for the sample, which are assigned to the lattice planes of (111), (200), and (220) of cubic Cu (JCPDS No.01-070-3039), revealing that the sample contains CuO, Cu_2O and Cu. With further increase of $N_2H_4 \cdot H_2O$ amount up to 3.5 mL or 5.0 mL, the XRD patterns show that the obtained samples contain Cu_2O and Cu or pure metallic Cu. The nanocrystal sizes of CuO, Cu_2O, and Cu for each sample were calculated using the Scherrer formula based on the diffraction peaks at 2θ values of 35.5°, 36.7,°and 43.3°, respectively, and these data are compiled in Table 1. For bare CuO, the nanocrystal has a mean size of 18 nm, while in the samples of CuO-Cu_2O and CuO-Cu_2O-Cu, the nanocrystal size of CuO is decreased from 18 to 17 nm. On the other hand, the nanocrystal size of Cu_2O in CuO-Cu_2O is 45 nm, which is smaller than that in CuO-Cu_2O-Cu (51 nm) but slightly larger than that in Cu_2O-Cu (41 nm). Different from CuO and Cu_2O, the nanocrystal size of Cu in CuO-Cu_2O-Cu (35 nm), Cu_2O-Cu (46 nm), and Cu (51 nm) is increased progressively with the increasing amount of $N_2H_4 \cdot H_2O$. We once treated CuO

nanoparticles by partial reduction in H_2/N_2 mixed gas with the purpose to obtain the multicomponent Cu-based catalysts, and also observed this trend of size change.[19]

Fig. 2b shows the TG curves of all the samples measured in air. It is seen that there is no visible weight change for CuO sample, suggesting the formation of nearly pure CuO phase. The CuO-Cu_2O sample shows a weight increase of 4.5 wt% in a wide temperature range (200-420 ^oC) which is derived from the oxidation of Cu_2O to CuO. Thus, the estimated content of Cu_2O in this sample is about 40.2 wt%. On the other hand, the CuO-Cu_2O-Cu and Cu_2O-Cu samples exhibit 11.2 and 17.1 wt% weight increase, respectively, corresponding to the oxidation of Cu_2O and Cu to CuO. In the case of Cu, the weight increase reaches 25.2 wt%, close to the theoretical value of the oxidation of Cu into CuO (25.0 wt%), confirming that it is metallic Cu.

Fig. 2c shows the H_2-TPR curves of all the samples. The hydrogen consumption peak areas (S_{TPR}) and peak temperatures (TM) are summarized in Table 1. As observed, with the decrease of the CuO content in the samples following the order of CuO, CuO-Cu_2O, CuO-Cu_2O-Cu, Cu_2O-Cu and Cu, the reduction temperature and hydrogen consumption are also slightly decreased. For the reduced samples, the reduction peaks move slightly to a lower temperature region with the increase of amount of reducing agent. Using the ratio of hydrogen consumption peak area to the mole number of O in CuO as the reference and based on the above TG analysis, it can calculate that the content of CuO in CuO-Cu_2O and CuO-Cu_2O-Cu samples is about 59.4 and 15.7 wt%, respectively. For Cu_2O-Cu, the content of Cu_2O is 40.6 wt%. Therefore, the above results indicate that the contents of Cu, Cu_2O, and CuO in the final products can be well tuned by adjusting the amount of $N_2H_4 \cdot H_2O$ in the preparation.

The high-resolution XPS spectra in Fig. 2d show the binding energies of Cu 2p3/2. The peaks at

934.2 eV are characteristic of Cu (II), whereas the ones at 932.9 eV are attributed to Cu (0) or Cu (I).[21,22] Unfortunately, from XPS data alone, it is difficult to distinguish clearly the Cu (0) and Cu (I) species due to the effects of crystal size and surface coverage on the binding energy.[23] However, by combining with the XRD results shown in Fig. 2a, we can judge whether the sample contains Cu (0) or Cu (I), or both of them. In other words, we can conclude that the sample actually contains CuO, Cu_2O and Cu.

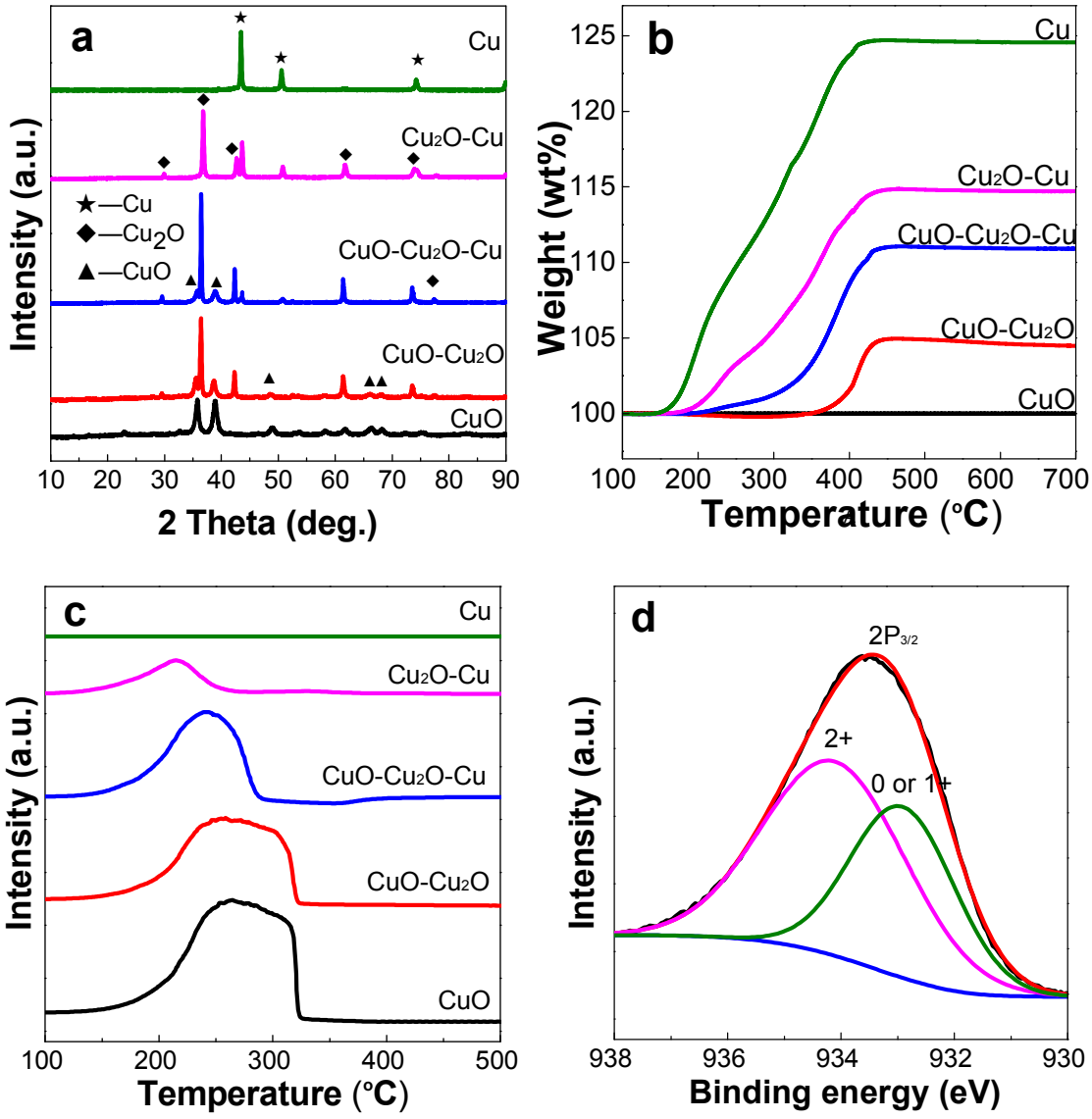

Fig. 2 XRD patterns (a), TG curves (b), and H_2-TPR curves (c) of all the samples, and XPS spectra of Cu 2p for the CuO-Cu_2O-Cu sample (d).

Table 1 The physical chemistry parameters of all the samples

Samples	Cu[a] (nm)	Cu_2O[a] (nm)	CuO[a] (nm)	Weight increase[b] (wt%)	TM[c] (^oC)	S_{TPR}[c]	S_{BET}[d] (m^2/g)
CuO	-	-	18	-	264.2	53460.8	15.3
CuO-Cu_2O	-	45	18	4.5	258.5	34482.3	10.2
CuO-Cu_2O-Cu	35	51	17	11.2	241.2	23146.7	3.6
Cu_2O-Cu	46	41	-	17.1	214.5	9435.0	3.4
Cu	51	-	-	25.2	-	-	2.5

[a]Calculated from the XRD patterns, standard errors: crystal size, 0.5 nm.

[b]Given by TG analysis.

[c]Obtained from H_2-TPR curves using integrated areas under curves presented.

[d]Calculated with BET method.

Fig. 3 shows the SEM images of all the samples. In agreement with the XRD results, the samples all appear to be well crystallized. Fig. 3a presents the SEM image of the CuO, which reveals that the sample is made up of a large quantity of different sheet-like submicrometer structures. However, after addition of a small amount of $N_2H_4 \cdot H_2O$, the SEM image shows that the obtained CuO-Cu_2O sample is composed of premature polyhedron structures, on the surface of which are covered with sheet-like substance (Fig. 3b), implying that the CuO crystallites are partially reduced to Cu_2O and attached to the surface simultaneously during the growth of the polyhedron structures, which is coincide with the previous studies.[24-26] A further increase in the amount of $N_2H_4 \cdot H_2O$ leads the obvious changes in the morphology of CuO-Cu_2O-Cu (Fig. 3c), which consist of sphere, cube, octahedron and other polyhedral with the size ranging from approximately 0.05-2 μm. Fig. 3d displays the SEM image of Cu_2O-Cu, in which the majority of the crystals have the cube and octahedron shapes, and their sizes are in the range of 100-500 nm. The Cu sample as shown in Fig.

3e exhibits a block–like shape with the size range of 0.1-3 μm.

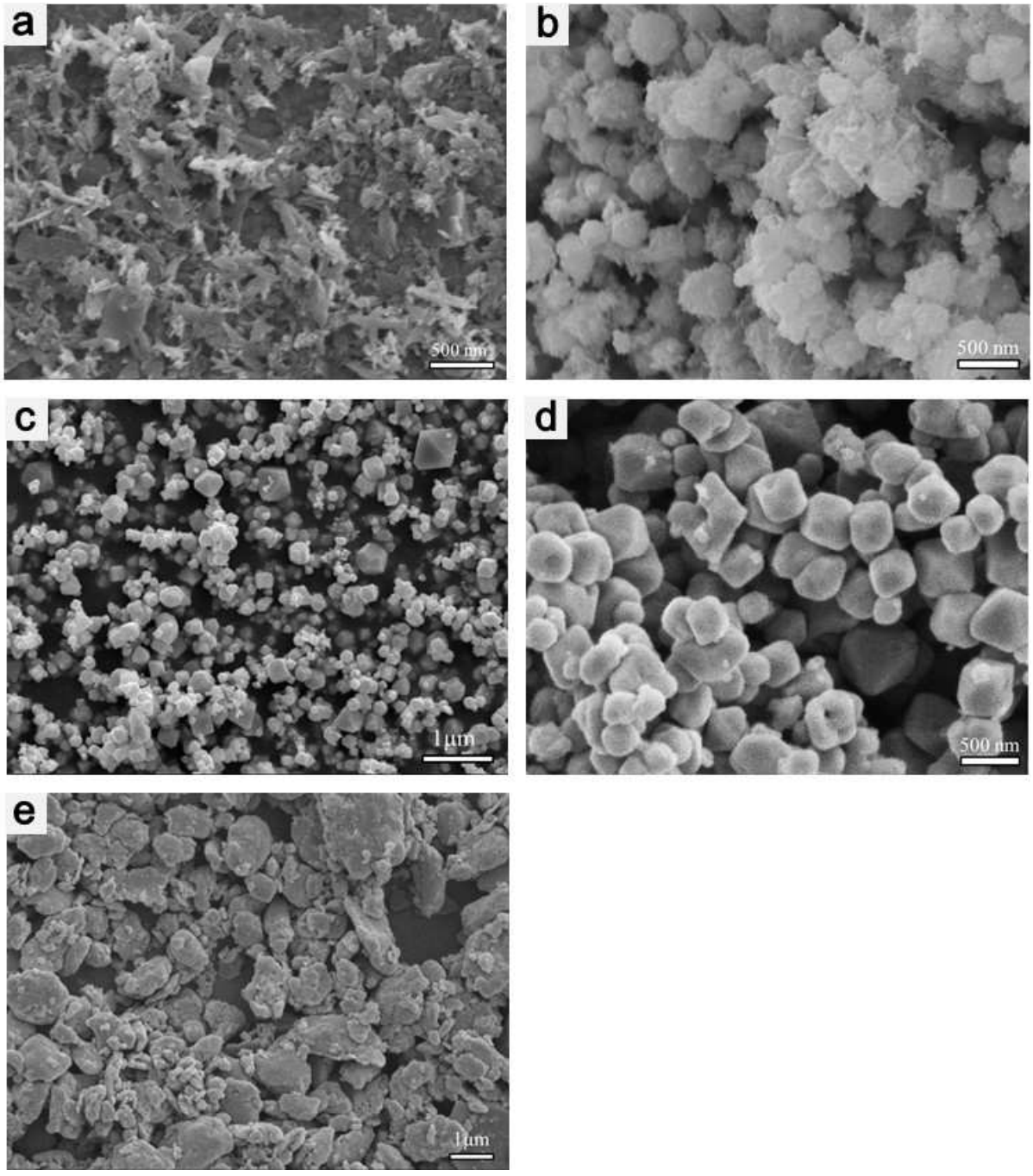

Fig. 3 SEM images of CuO (a), CuO-Cu_2O (b), CuO-Cu_2O-Cu (c), Cu_2O-Cu (d), and Cu (e).

Fig. 4a presents the TEM image of the CuO-Cu_2O-Cu sample, which consists of cube, octahedron, sphere and other polyhedral, in full agreement with the above SEM result (Fig. 3c). The

high-resolution transmission electron microscope (HRTEM) image of CuO-Cu_2O in Fig. 4b shows the presence of two different interplanar distances of 0.25 and 0.24 nm, corresponding to the (111) planes of CuO and Cu_2O, respectively. Moreover, two sets of diffraction spots in the fast Fourier transform (FFT) patterns further verify the coexistence of the two structures. Similarly, the CuO-Cu_2O-Cu sample (Fig. 4c) possesses three apparent lattice spacings, in which the one at 0.21 nm corresponds to the (111) plane of Cu, and the other two indexed to the (111) planes of CuO and Cu_2O remain the same (0.25 and 0.24 nm) as CuO-Cu_2O. In the case of Cu_2O-Cu (Fig. 4d), two lattice plane distances of 0.24 and 0.21 nm are observed, which are characteristic of the (111) facets of Cu_2O and CuO, respectively. These results prove that the prepared Cu-based samples are composed of polycrystals, while within each multi-component particle there are different Cu component crystals, supporting the successful synthesis of Cu-based catalysts with controllable composition by varying the amount of reducing agent using the wet chemical method.

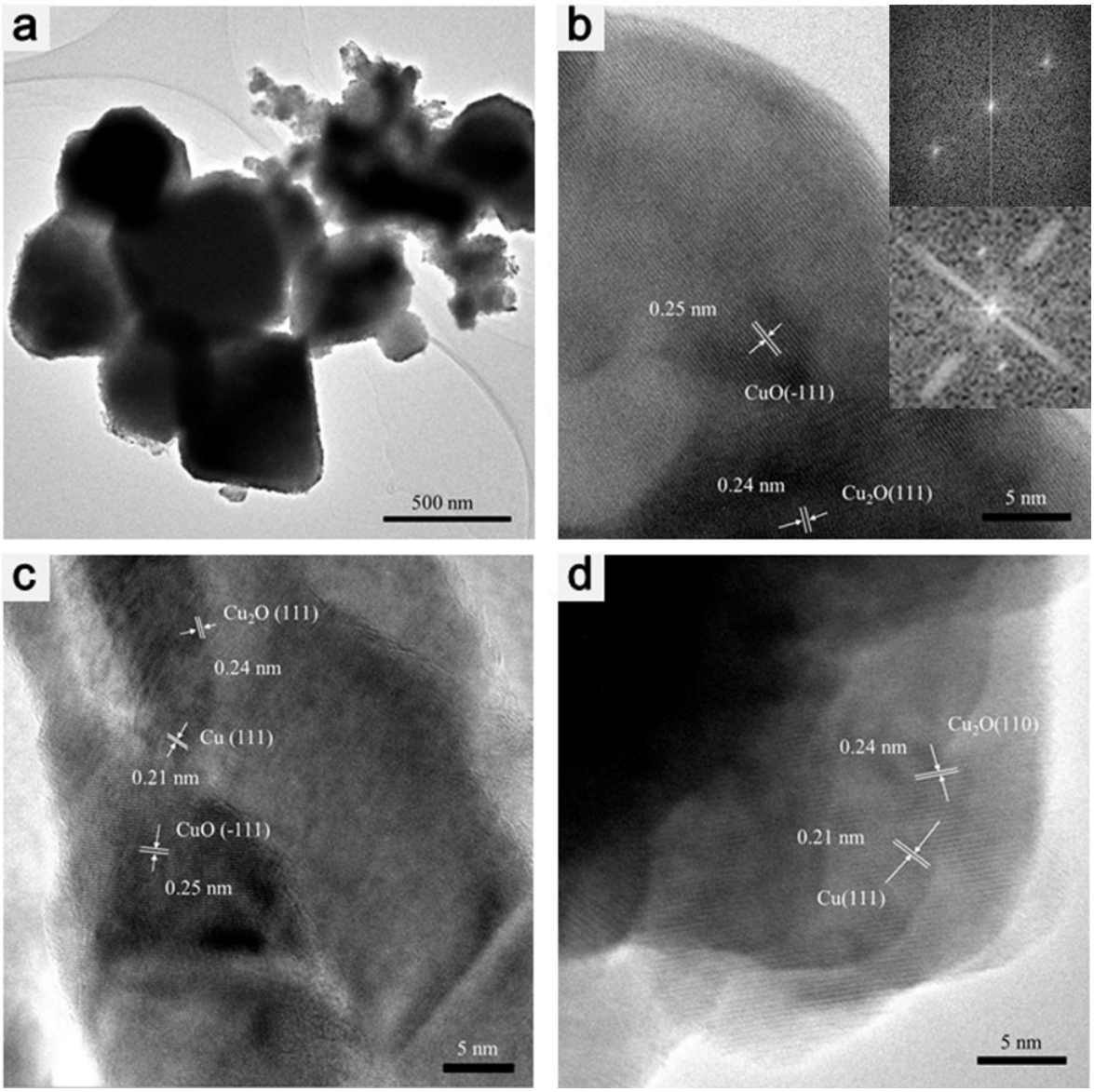

Fig. 4 TEM image of CuO-Cu_2O-Cu (a), HRTEM images of CuO-Cu_2O (Top and down insets show the corresponding FFT pattern of CuO (-111) and Cu_2O (111), respectively) (b), CuO-Cu_2O-Cu (c), and Cu_2O-Cu (d).

3.2. Reduction Mechanism.

The reactions involved in the CuO synthesis and their reduction process are shown in the following equations:

$$CuSO_4 + 2NaOH \rightarrow Cu(OH)_2 + Na_2SO_4 \quad (3)$$

$$Cu(OH)_2 \rightarrow CuO + H_2O \quad (4)$$

$$CuO + N_2H_4 \rightarrow 2Cu_2O + N_2 + 2H_2O \quad (5)$$

$$Cu_2O + N_2H_4 \rightarrow 2Cu + N_2 + H_2O \quad (6)$$

The chemical reaction between $CuSO_4$ and NaOH yields cupric-hydroxide ($Cu(OH)_2$) (Formula (3)), which is a metastable phase. Upon the heating in a constant-temperature (70 ^oC) water bath under magnetic stirring, it is decomposed into more stable cupric-oxide (CuO) (Formula (4)),[27] which has been also confirmed previously by Cudennec and Lecerf et al.[28] Upon addition of $N_2H_4 \cdot H_2O$, which is employed as a reducing agent, CuO is reduced into Cu_2O and Cu, accompanying with production of N_2 and H_2O (formulas (5) and (6)).[24,25] In addition, we also found that a trace of NH_3 as a by-product will also be generated. The formation of various products with distinct morphologies is illustrated in Scheme 1. As mentioned above, $Cu(OH)_2$ is not stable. When heated at 70 ^oC for 10 min, it is transformed into black CuO solely, which has the sheet-like morphology and submicrometer size. Upon addition of a small amount of $N_2H_4 \cdot H_2O$, an obvious change in the product morphology and size is observed (Fig. 3b in SEM image). Clearly, there should be a dissolution-recrystallization process starting from the solid precursor.[26] During the reduction process, the added $N_2H_4 \cdot H_2O$ reacts with the free Cu^{2+} ions via coordination and reduction steps. With progressive dissolution of CuO to yield Cu^{2+} and subsequent reduction of Cu^{2+} to Cu^+, the CuO particles are gradually dissolved and recrystallization.[25,26] When the amount of $N_2H_4 \cdot H_2O$ reaches 1.5 ml, part of CuO is transformed into Cu_2O, forming nanocrystals of both CuO and Cu_2O with premature polyhedron structures. Continuously increasing the amount of $N_2H_4 \cdot H_2O$ to 2.5 ml, CuO is completely transformed into Cu_2O, and even part of the yielded Cu_2O is further converted into Cu. Thus, a coexistence of CuO, Cu_2O, and Cu grains with the structure of sphere, cube,

octahedron and other polyhedral is obtained. It should be noted that the presence of small amounts of ions such as Na^+, OH^-, etc. has a great influence on the morphology of Cu_2O product.[26] Finally, with a further increase of $N_2H_4 \cdot H_2O$ amount to 3.5 ml or 5.0 ml, as there is surplus of reducing agent, the generated Cu_2O is converted into Cu_2O-Cu or pure Cu totally. Therefore, by tuning the supply of $N_2H_4 \cdot H_2O$, it is able to control the content of CuO, Cu_2O, and Cu in the final Cu-based products, as proved by above comprehensive characterizations with XRD, TG, TPR, XPS and TEM techniques.

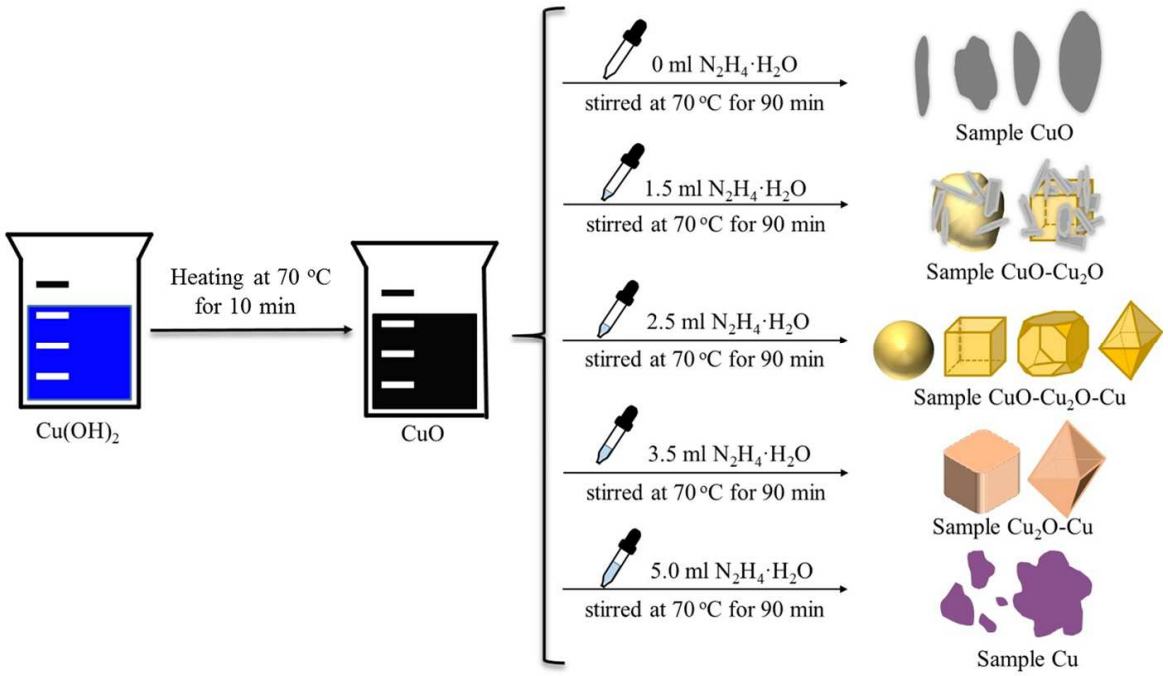

Scheme 1 Graphic description for the reduction mechanism.

3.3. Catalytic property of Cu-based catalysts

Table 2 summarizes the catalytic performance of all the samples for M2 synthesis via the Rochow reaction. As shown, the CuO sample achieves a M2 selectivity of 66.1% and Si conversion of 26.4%. For CuO-Cu_2O, the corresponding values become 68.7 and 27.2%, respectively. In the case of CuO-Cu_2O-Cu, a markedly improved M2 selectivity of 80.0% and Si conversion of 51.4% are achieved, higher than those of Cu_2O-Cu (71.8% M2 selectivity and 32.0% Si conversion). For

sole Cu, both the M2 selectivity and the Si conversion are decreased obviously again. Also, the characterization data of the reaction product organo silanes via GC are provided (See Table S1-S5 and Fig. S1-S5 in Supporting Information). It should be pointed out that the error bars for both conversion and selectivity were ±0.1% and all the catalytic data were obtained by at least three repeated experiments using the same silicon. As we known, M2 is the most desirable monomer in organosilane industry, the above results demonstrate that the prepared catalysts possessing three components of Cu, Cu_2O, and CuO have the best M2 selectivity and yield among all the samples, probably because of the synergistic effect among Cu, Cu_2O, and CuO, which promotes the catalytic activity for the Rochow reaction.[5] In addition, byproducts such as M1, M3, M1H, M2H, LB, and HB with a negligible difference over the different prepared catalysts are also detected except that on the Cu sample.

Table 2 Catalytic performances of all the catalysts for Rochow reaction[a]

Samples	Product Composition (%)								
	M1	M2	M3	M1H	M2H	LBR	HBR	M2 yield	C-Si (%)
CuO	12.5	66.1	1.4	14.9	0.8	0.3	4.0	17.5	26.4
CuO-Cu_2O	11.3	68.7	1.0	9.2	0.4	0.4	9.0	18.7	27.2
CuO-Cu_2O-Cu	10.1	80.0	1.5	7.2	0.9	0.1	0.2	41.1	51.4
Cu_2O-Cu	11.4	71.8	1.0	11.2	1.1	0.1	3.4	23.0	32.0
Cu	21.9	47.3	1.0	23.0	0.9	0.3	5.6	8.8	18.7

[a] Reaction conditions: cat., 1.0 g; catalyst: Si (mass ratio)= 1:10; flow rate of CH_3Cl, 25 mL min^{-1}; temp., 325 ^oC; time, 24 h.

Fig. 5 displays the XRD patterns of the waste contact masses after reaction, which contain the unreacted Si, the Cu-based catalyst, and trace amount of promoter Zn. As shown in Fig. 5a, all the

waste contact masses are composed of Si and Cu, but lack of Cu_2O and CuO species. The formation of Cu may originate from the reaction of MeCl with the lattice oxygen of the Cu-based catalyst.[9] An enlarged view of the XRD patterns in the range of 40-50° (Fig. 5b) shows the presence of η-Cu_3Si and $Cu_{6.69}Si$ species, suggesting the formation of alloyed Cu_xSi active components by reaction of Cu and Si via diffusion during the reaction. The Cu_3Si alloy, generally produced between the Cu catalyst and the Si interface at elevated temperatures,[29] is normally regarded as the key catalytic active species in the Rochow reaction,[30,31] by which Methylchlorosilanes (MCSs), especially M2, are formed. The amounts of Cu_3Si can substantially affect the Si conversion and M2 selectivity.[6] The intensity of Cu_3Si peaks observed for CuO-Cu_2O-Cu is much higher than that of the other samples, suggesting that CuO-Cu_2O-Cu is more active in generating Cu_3Si than the other samples. This may be because the ternary composition of CuO-Cu_2O-Cu has a stronger synergistic effect and closer contact between the catalysts and the solid Si, thus promoting the formation of more active Cu_3Si phases, which is the key step to enhance the catalytic activity for M2 production.

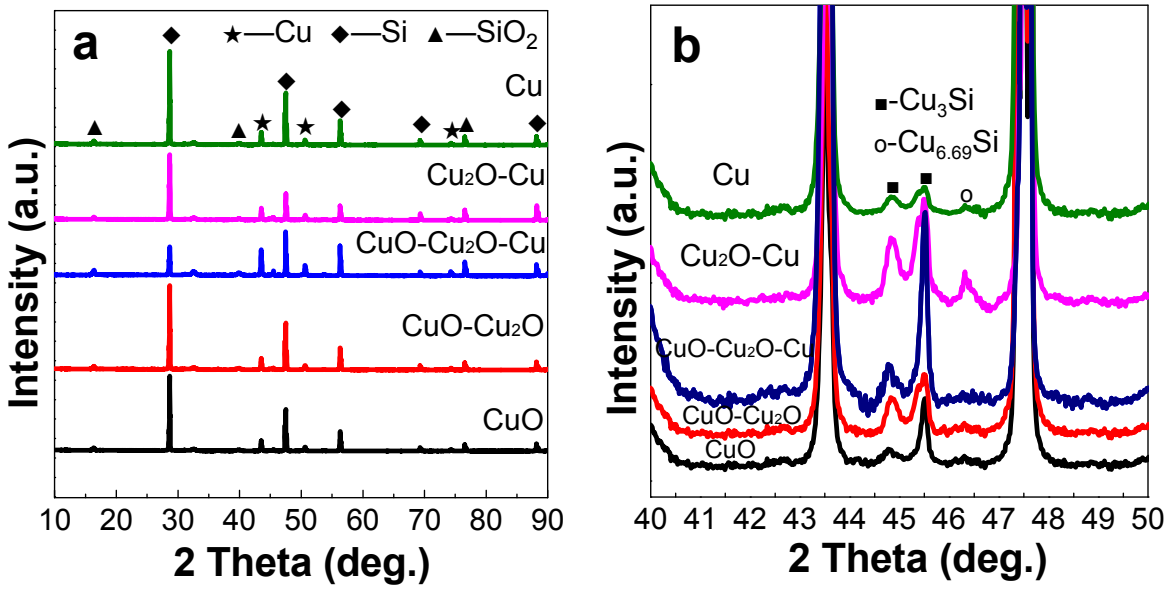

Fig. 5 XRD patterns of waste contact masses (a) and enlarged view in the 2θ range of 40-50° (b).

Fig. 6a shows the SEM images of the Si particles after the reaction using CuO-Cu_2O-Cu as the catalyst. The smooth region on the surface of Si particle stems from the unreacted Si, while coarse or cavity-like region from reacted Si, suggesting the occurrence of etching process during the reaction, consistent with the so-called anisotropic etching reaction mechanism.[14] The element mapping images show the distribution of the elements Si (Fig. 6b), Cu (Fig. 6c) and C (Fig. 6d) on the surface of the waste contact mass. The element Si mapping image clearly shows the reacted (dark yellow) and unreacted (bright yellow) zones of Si particle, while both Cu (dark cyan) and C (red) distribute uniformly on the reacted or etched Si surface, indicating the occurrence of catalytic reaction between Si particles and Cu-based catalysts. As shown in Scheme 2, a mechanism for catalytic cycle is proposed. The ternary Cu-Cu_2O-CuO catalyst is first transformed to Cu* (active species) via the reaction of MeCl with the lattice oxygen, which then reacts with Si to form alloyed Cu_xSi active intermediate. Further, MeCl is adsorbed on their surface and transformed into M2, and meanwhile Cu* is released again.

The above results allow us to describe graphically the possible Rochow reaction process in the presence of Cu-based catalyst (Scheme 3). First, Si is mixed with the reduced Cu particles in submicrometer size before the reaction. With diffusion of Cu into the Si, the Cu_xSi alloy is gradually formed at the Cu catalyst and the Si interface at the elevated temperatures, which further reacts with the gas MeCl to form MSCs. As the reaction proceeds further, more elemental copper is produced while the Cu in the Cu_xSi alloy is reduced until the deactivation of the catalyst. At the same time, MeCl may be transformed into carbon deposition (C) initiated by the metallic Cu, leading to the deactivation of the contact mass. The presence of the multicomponent particles structure should enhance the gas diffusion into the Cu-Si contact area, resulting in the formation of much more active

species. Nevertheless, the real synergistic effect is not yet fully understood at present and should be further explored.

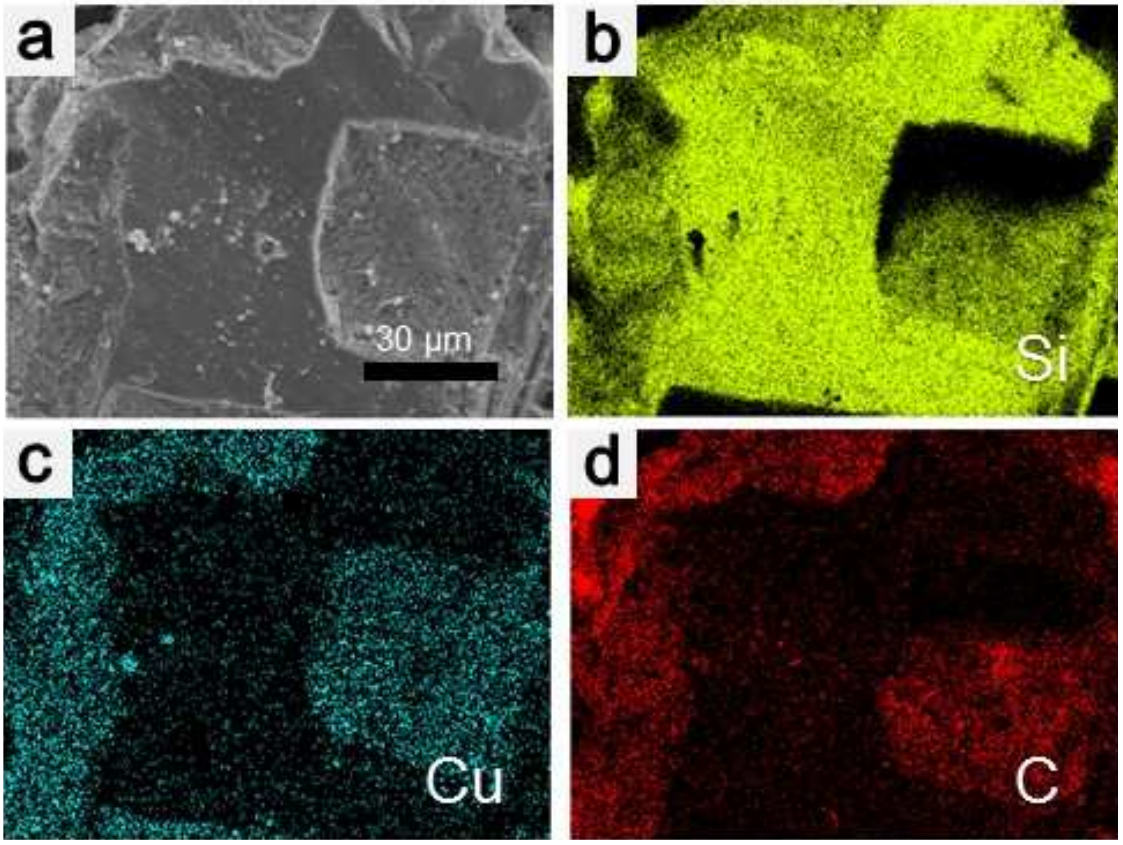

Fig. 6 SEM images of Si particle after reaction (a), elemental mapping images of Si (b), Cu (c) and C (d).

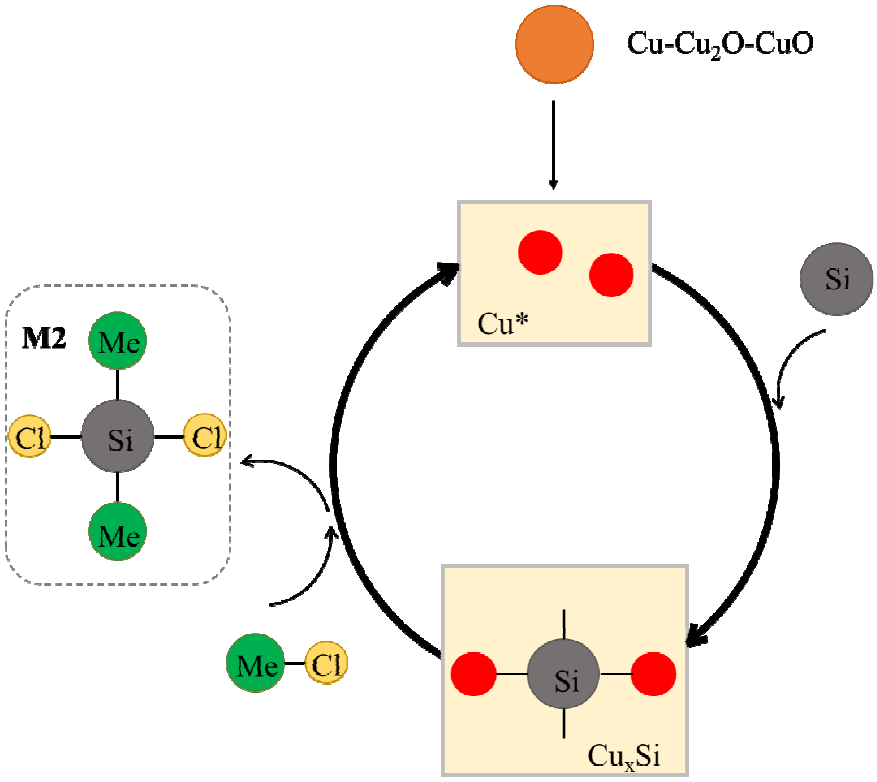

Scheme 2 A proposed catalytic mechanism for catalytic cycle.

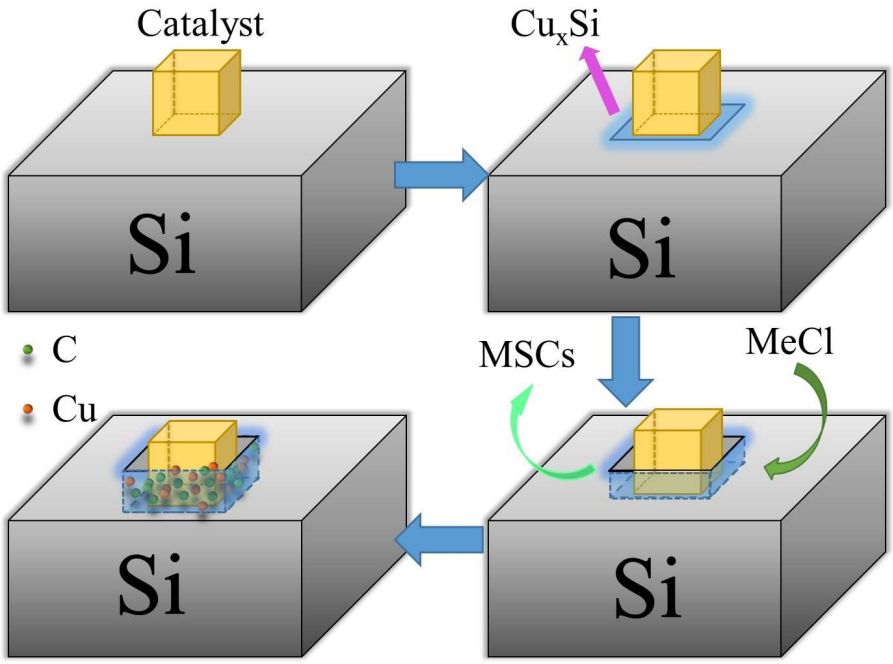

Scheme 3 Schematic illustration of the process of Rochow reaction.

This method is simple without use of any complicated and delicate equipment, and the reaction conditions are mild, as the reaction temperature is 70 °C only. More importantly, this method is readily scalable. Our experiment results showed that about 10 g of products could be obtained at one time by using a 500 mL beaker (not shown), indicating its great potentiality for industrial application.

4. Conclusions

In summary, we have demonstrated the controllable synthesis of the Cu-based catalysts with variable CuO, Cu_2O and Cu contents by a wet chemical method, in which the key is to control the amount of $N_2H_4 \cdot H_2O$ used as the reducing agent. Various characterizations indicate that the reduction of CuO is a successive reaction that yields Cu_2O, and Cu, which in turn provides the possibility to finely tune the catalyst composition via varying the amount of reducing agent. Comparing with the synthesized CuO and Cu particles, the multicomponent CuO-Cu_2O-Cu catalyst shows much higher M2 selectivity and Si conversion in the Rochow reaction, proving the significance of the synergistic effect among the multicomponent. It is expected that this ternary CuO-Cu_2O-Cu catalysts will have great potential in the industrial Rochow reaction.

Acknowledgements

The authors gratefully acknowledge the financial supports from the National Natural Science Foundation of China (no. 51272252and21206172). Z. Z is grateful to the kind supports of both Nanyang Technological University (NTU) and Institute of Chemical Engineering and Sciences (ICES) under Agency for Science, Technology and Research (A*STAR).

Supplementary material

Supplementary data associated with this article can be found, in the online version, at…

References

1 E. G. Rochow, *J. Am. Chem. Soc.*, 1945, **67**, 963-965.

2 A. D. Gordon, B. Hinch and D. R. Strongin, *Catal. Lett.*, 2009, **133**, 14-22.

3 H. Lieske and R. Zimmermann, *Catal. Lett.*, 1995, **33**, 413-420.

4 L. Zhang, S. Hao, C. H. Yang, J. Li, K. Yang, C. F. Hu and S. B. Ge, *Appl. Organomet. Chem.*, 2011, **25**, 508-513.

5 Z. L. Zhang, H. W. Che, Y. L. Wang, J. J. Gao, L. R. Zhao, X. L. She, J. Sun, P. Gunawan, Z. Y. Zhong and F. B. *Su*, *Ind. Eng. Chem.*, 2012, **51**, 1264-1274.

6 L. N. Lewis and W. J. Ward, *Ind. Eng. Chem.*, 2002, **41**, 397-402.

7 D. H. Sun, B. E. Bent, A. P. Wright and B. M. Naasz, *J. Mol. Catal. A: Chem.*, 1998, **11**, 169-183.

8 D. H. Hashiguchi, R. J. Dietrich and G. P. Schoepe, *US Patent* 4504596, 1985.

9 L. N. Lewis, W. V. Ligon and J. C. Carnahan, *Silicon Chem.*, 2002, **1**, 23-33.

10 A. D. Gordon, B. Hinch and D.R. Strongin, *J. Catal.*, 2009, **266**, 291-298.

11 K. H. Brookes, M. R. H. Siddiqui, H. M. Rong, R. W. Joyner and G. J. Hutchings, *Appl. Catal. A: Gen.*, 2001, **206**, 257-265.

12 Y. X. Zhu, Y. L. Wang, L. Y. Song, X. Chen, W. Y. Liu, J. Sun, X. L. She, Z. Y. Zhong and F. B. Su, *RSC Adv.*, 2013, **3**, 9794-9802.

13 Z. L. Zhang, H. W. Che, Y. L. Wang, X. L. She, J. Sun, P. Gunawan, Z. Y. Zhong and F. B. Su, *ACS Appl.Mater. Interfaces*, 2012, **4**, 1295-1302.

14 Z. L. Zhang, H. W. Che, J. J. Gao, Y. L. Wang, X. L. She, J. Sun, P. Gunawan, Z. Y. Zhong and F. B. Su, *Catal. Sci. Technol.*, 2012, **2**, 1207-1212.

15 Z. L. Zhang, H. W. Che, Y. L. Wang, L. Y. Song, Z. Y. Zhong and F. B. Su, *Catal. Sci. Technol.*, 2012, **2**, 1953-1960.

16 Z. L. Zhang, H. W. Che, J. J. Gao, X. L. She, J. Sun, Z. Y. Zhong and F. B. Su, *RSC Adv.*, 2012, **2**, 2254-2256.

17 X. Chen, L. H. Jia, Y. L. Wang, L. Y. Song, Y. X. Zhu, W. Y. Liu, Z. Y. Zhong and F. B. Su, *J. Colloid Interface Sci.*, 2013, **404**, 16-23.

18 M. Khitouni, R. Daly, M. Mhadhbi and A. Kolsi, *J. Alloys Compd*, 2009, **475**, 581-586.

19 W. Y. Liu, L. H. Jia, Y. L. Wang, L. Y. Song, Y. X. Zhu, X. Chen, Z. Y. Zhong and F. B. Su, *Ind. Eng. Chem.*, 2013, **52**, 6662-6668.

20 S. M. Liu, Y. L. Wang, Y. X. Zhu, G. N. Wang, Z. L. Zhang, H. W. Che, L. H. Jia and F. B. Su, *RSC Adv.*, 2014, **4**, 7826-7833.

21 F. Capece, V. D. Castro, C. Furlani, G. Mattogno, C. Fragale, M. Gargano and M. Rossi, *J. Electron. Spectrosc. Relat. Phenom.*, 1982, **27**, 119-128.

22 H. Tolentino, F. Baudelet, A. Fontaine, T. Gourieux, G. Krill, J. Henry and J. Rossat-Mignod, *Physica C*, 1992, **192,** 115-130.

23 K. J. Ziegler, R. C. Doty, K. P. Johnston and B. A. Korgel, *J. Am. Chem. Soc.*, 2001, **123**, 7797-7803.

24 W. Z. Wang, O. K. Varghese, C. M. Ruan, M. Paulose and C. A. Grimes, *J. Mater. Res.*, 2003, **18** 2756-2759.

25 A. Muramatsu and T. Sugimoto, *J. Colloid Interface Sci.*, 1997, **189**, 167-173.

26 J. W. Zhu, H. P. Bi, Y. P. Wang, X. Wang, X. J. Yang and L. D. Lu, *Mater. Lett.*, 2008, **62**, 2081-2083.

27 J. P. Li, F. Q. Sun, K. Y. Gu, T. X. Wu, W. Zhai, W. S. Li and S. F. Huang, *Appl. Catal.*, 2011, **406**, 51-58.

28 Y. Cudennec and A. Lecerf, *Solid State Sci.*, 2003, **5**, 1471-1474.

29 N. Floquet, S. Yilmaz and J. L. Falconer, *J. Catal.*, 1994, **148**, 348-368.

30 E. Gaffet and F. Bernard, *Ann. Chim. - Sci. Mat.*, 2002, **27**, 47-59.

31 D. H. Sun, B. E. Bent, A. P. Wright and B. M. Naasz, *Catal. Lett.*, 1997, **46**, 127-132.